Korean J. Chem. Eng., 39(4), 902-912 (2022)
DOI: 10.1007/s11814-022-1085-4

pISSN: 0256-1115
eISSN: 1975-7220

Flow analysis and development of a model to simulate transient temperature of hydrogen from pre-cooler to on-board storage tank during hydrogen refueling

Byung Heung Park*,† and Dong Hoon Lee**

*Department of Chemical and Biological Engineering, Korea National University of Transportation, 50 Daehak-ro, Chungju-si, Chungcheongbuk-do 27469, Korea
**Korea Gas Safety Corporation, 1390 Wonjung-ro, Maengdong-myeon, Eumseong-gun, Chungcheongbuk-do 27738, Korea
(*Received 26 October 2021 • Revisedc 13 January 2022 • Accepted 9 February 2022*)

Abstract−Hydrogen energy is expected to play an important role in energy transition policies. Currently, the utilization of hydrogen energy is mainly in the field of mobility associated with fuel cell electric vehicles (FCEVs). To increase the utilization of FCEVs, it is essential to develop a method for safely refueling hydrogen into on-board storage tanks which have a temperature limitation. Therefore, it is necessary to understand the flow and heat transfer characteristics of hydrogen to keep the temperature lower than the limitation. In this study, a model for predicting the temperature of hydrogen at the pipeline outlet was developed based on flow characteristics analysis. It is revealed that the flow in a pipeline can be considered as incompressible and that the turbulence model can be applied with respect to pressure, temperature, and pipeline diameter. The proposed model is based on energy balances of the pipeline and the flowing hydrogen. Analogous methods are compared to obtain heat transfer coefficient required for thermal analysis. Although there is a difference in the heat transfer coefficient with respect to the analogous methods, little difference is found in the hydrogen temperature. Additionally, it is found that the equivalent length can be used to account for the thermal mass of the pipeline and the experimental results can be accurately simulated using a relatively large external heat transfer coefficient.

Keywords: Hydrogen, Hydrogen Refueling, Flow Analysis, Heat Transfer Coefficient, Numerical Analysis

INTRODUCTION

The Republic of Korea (ROK) is moving forward to become a global leader in a hydrogen-based economy. In January 2019, the government announced its Hydrogen Economy Roadmap, setting out its targets to 2040 [1]. The roadmap calls for increasing the number of fuel-cell electric vehicles (FCEVs) to 5.9 million as well as hydrogen refueling stations (HRSs) to 1,200 by 2040. The roadmap also addresses goals on various kinds of FCEVs in a mobility application, which includes passenger vehicles, buses, taxis, and trucks.

In July 2020, the Korean government also announced the Green New Deal aimed at accelerating the transition from a carbon-dependent economy to a low-carbon economy. Although the Green New Deal is an economic policy, it is closely related to the hydrogen industry since FCEVs produce nearly zero exhaust gas and reduce greenhouse gas emissions. Hydrogen will play a key role in the policy and the government set a target of 200,000 FCEVs on domestic roads by 2025 as a part of the Green New Deal [2].

The achievement of the goals on the number of FCEVs should be supported by technical development on refueling. Consumers expect on FCEVs what they have experienced while driving internal combustion engine vehicles (ICEVs). Therefore, the most important characteristics of FCEVs are a long driving distance and a short refueling time comparable to ICEVs. To provide an experience similar to that of ICEVs, hydrogen refueling protocols have been developed to enable stations to safely and rapidly fill FCEVs. Hydrogen refueling protocol is a set of procedures that control the process to fill a compressed hydrogen storage system (CHSS). Currently, SAE J2601 is the worldwide recognized refueling protocol standard for light duty vehicles (LDVs) [3]. It is applied within a capacity range between 50 and 250 L, which corresponds to 2 and 10 kg of fuel weight, respectively, when hydrogen is compressed to 70 MPa at 15 °C. All the methodologies for refueling LDVs in SAE J2601 are restricted to a maximum mass flow rate of 60 g/s. In 2020, the revision of SAE J2601 extended the capacity range by giving no formal upper limit. However, the limitation of 60 g/s was still imposed on the mass flow rate.

Currently, the majority of heavy duty vehicles (HDVs), such as buses and trucks, are powered by diesel engines [4]. To achieve comparable refueling for HDVs of ICEVs, FCEVs should be filling 10 to 40 kg of hydrogen in 5 to 7 min. As for HDVs, SAE J2601-2 [5] addresses safety limit and performance requirements introducing fueling at flow rates up to 120 g/s. Contrary to SAE J2601, SAE J2601-2 is not prescriptive and specifies only what conditions or parameters to avoid for safe refueling. SAE J2601-2 presents very little guidance on how to fill CHSSs in HDVs and, instead, focuses on the boundary conditions of refueling as well as process limits to avoid an impact on safety.

When hydrogen gas is introduced into CHSS, the hydrogen gas

†To whom correspondence should be addressed.
E-mail: b.h.park@ut.ac.kr

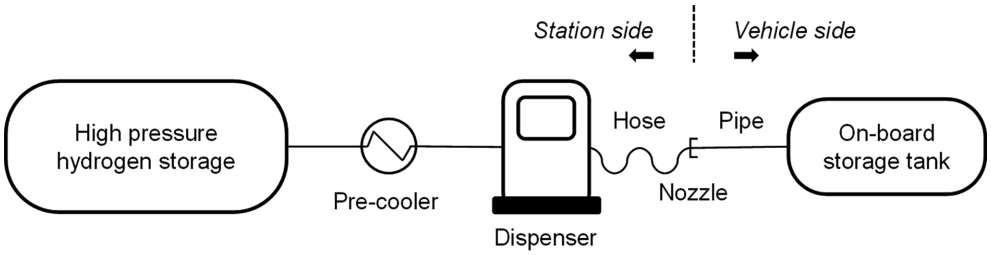

Fig. 1. Schematic diagram of typical connection from HRS to FCEV.

temperature inside the tank rises due to heat of compression and heat exchange with ambient atmosphere through components of fueling lines such as hoses, nozzles, and receptacles. Accordingly, the temperature of the tank also rises, but it should be maintained under the limitation of 85 °C for type IV tank. When the temperature exceeds the limit, the refueling process is forcibly aborted to ensure the safety of the storage tank.

Recently, many researches have been implemented to understand and analyze the gaseous hydrogen refueling process. Early studies were mainly about hydrogen storage density and the performance of hydrogen storage systems [6-9]. Thereafter, with the commercialization of compressed hydrogen storage devices, the focus was shifted to composite storage cylinders [10], rapid refueling of tanks [11], and performance of the refueling process [12]. Numerous investigations on experiments and simulations on refueling compressed hydrogen have been reported for various volumes of tanks. The final storage density at the end of hydrogen filling was measured at the gas testing facility at the Joint Research Centre (GasTef JRC) [13-15], Air Liquid [16], and the National Research Council of Canada's Institute for Fuel Cell Innovation [17]. Simulation studies were mainly carried out to estimate the end temperature and temperature distribution inside the storage tank [18], thermal behavior of compressed hydrogen [19,20], and heat losses [21].

Some thermodynamic models [22-25] have been developed by coupling an energy balance for gas side with heat transfer for the wall of storage vessels. However, the effect on heat transfer was analyzed focusing on the hydrogen storage tank, and there were not many studies on the heat transfer occurring in the pipeline through which the pre-cooled hydrogen flows. Studies on the heat transfer coefficient have been also conducted centered on the hydrogen storage tank [26-28]. Analysis of the heat transfer coefficient, which is essential for the analysis of heat transfer occurring in the hydrogen pipe, has not been carried out regarding flow conditions.

The amount of heat added to gas before entering into a tank cannot be ignored when estimating gas temperature stored in the tank [29]. Therefore, thermal energy interaction between gas and pipeline should be included to develop a model describing the refueling process of hydrogen [30-32]. The thermal effect is closely related to mass flow rate. However, the focus has been on LDVs and only recently models for HDVs have been developed to numerically simulate the temperature rise during fast filling [33,34]. Internal convective heat transfer is taking place inside of the fueling line, which is governed by the mass flow rate. Therefore, hydrogen heat transfer of internal flow should be adequately described for the application to HDVs models.

In this work, first, the flow characteristics were analyzed to understand the fluid mechanics and the heat transfer occurring in the hydrogen flow. After investigating the incompressible flow conditions on temperature and pressure, a flow analysis was carried out to choose proper equations describing the pressure drop and the heat transfer coefficient. The equations were used to develop a model simulating hydrogen temperature at a pipeline outlet. Finally, the model parameters were determined to fit experimental data.

HYDROGEN REFUELING

Refueling stations for FCEVs dispense compressed hydrogen into a vehicle. Fig. 1 shows a schematic of a typical connection from a hydrogen refueling station (HRS) to an FCEV. A representative HRS consists of high-pressure storage tank, pre-cooler, and dispenser [35,36]. The hydrogen is pressurized enough to fill a vehicle up to 35 MPa (H35) or 70 MPa (H70) [37] and sits in a storage tank. The hydrogen is pre-cooled through a heat exchanger before it is introduced into a vehicle. Cooling prevents the vehicle's onboard tanks from overheating beyond the safety limit. The fueling dispenser controls and measures the flow rate in accordance with a target pressure. The hose of the dispenser is connected to a vehicle through a nozzle during refueling. The dispensed hydrogen passes through a pipeline inside the vehicle before entering the on-board tank. The pressure and temperature of the on-board storage tank are monitored by a control system of HRS.

SAE J2601 [3] defines HRS type as T40, T30, T20, and T0 with respect to capability of pre-cooling hydrogen gas. The temperature range for each type of HRS is set to be continuous (see Fig. 2), so even if the hydrogen temperature during refueling is out of the control temperature range for a certain period, the refueling process is not shut down but instead recedes to a reduced filling rate referred to as 'fall-back fueling'.

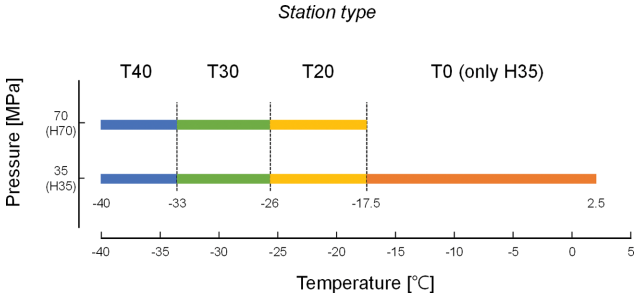

Fig. 2. Types of HRS regarding pre-cooling temperature range.

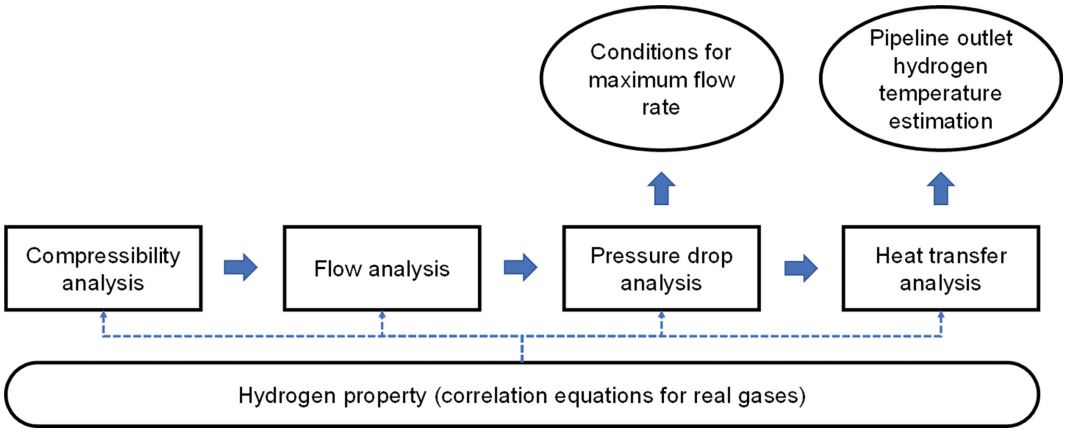

Fig. 3. Schematic description of analysis sequence for the temperature estimation at pipeline outlet.

SCHEME OF ANALYSIS ON HYDROGEN FLOW THROUGH PIPELINE

In general, the internal flow analysis of a gas is aimed at calculating the flow rate or estimating the pressure drop. In this work, the heat transfer phenomenon is the main object of analysis rather than the calculation of the flow rate because the hydrogen flowing from HRS to the on-board storage tank is heated by thermal interaction with a pipeline. The analysis of the fluid flow characteristics should be preceded since the heat transfer phenomenon is closely related to the flow characteristics of the fluid.

The analysis procedure performed in this study is schematically shown in Fig. 3. All the analysis steps for hydrogen filling are based on actual gas properties rather than ideal gas, considering very high-pressure conditions on FCEV refueling. First, the incompressible flow region is analyzed, and then the turbulent flow conditions are confirmed. The pressure conditions to obtain the maximum flow (60 g/s or 120 g/s) are estimated using a friction factor equation applied in the turbulent flow conditions. Finally, the heat transfer coefficient is estimated by applying analogous methods associated with the turbulent flow behavior to calculate the temperature of hydrogen at the pipeline outlet.

CHARACTERISTICS OF HYDROGEN FLOW IN REFUELING PROCESS

1. Equation of State (EOS)

Volumetric property estimation is of importance for understanding characteristics of a gas flow. It is well known that the real gases fail to follow the ideal gas law at high pressure because attractive forces between molecules become significant. In the pressure range up to 90 MPa, which is the typical condition of gaseous hydrogen in the high-pressure storage tanks at refueling stations, the equation of state of the ideal gas cannot be used to calculate hydrogen properties.

Currently, various equations of state (EOSs) are available for quantifying volumetric and thermal changes of hydrogen. Cubic EOSs are classical models for fluids, which have long been developed and improved since the 19th century. The van der Waals (vdW) equation and many modifications can be written as a generic cubic equation [38], which includes two or more related constants applicable to different real gases. Polynomial, Benedict-Webb-Rubin type, and Helmholtz-type EOSs associated with more than ten terms are also proposed considering isomers of hydrogen [39]. Many complex and more accurate EOSs have been devised to better represent pressure-volume-temperature (PVT) properties and vapor-liquid equilibrium (VLE). However, cubic EOSs are still actively used in chemical process design and simulation.

A comparative study [40] showed that Redlich-Kwong (RK) and Peng-Robinson (PR) families, which are cubic EOSs, can accurately predict compressibility factor, enthalpy, and heat capacity of hydrogen in the temperature and pressure range in compressed storage systems. In this regard, RK and PR EOSs without modification have been successfully applied to thermodynamic analysis [17,24, 25] as well as CFD simulations [30,41-44] of hydrogen refueling. Recently, a comparison of RK and PR [24,45] using reference data from NIST Chemistry Webbook [46] revealed that RK model fits the experimental data of molar volume as well as molar enthalpy of hydrogen better than PR model. Therefore, we utilized RK EOS, which is given as

$$P = \frac{RT}{(V-b)} - \frac{a}{V(V+b)} \tag{1}$$

where P, T, and V denote pressure, temperature, and molar volume, respectively. R is the universal gas constant and two component-dependent constants, a and b, are related to the critical properties through the following equations:

$$a = 0.42748\frac{R^2T_c^2}{P_c}\alpha \tag{2}$$

$$b = 0.08664\frac{RT_c}{P_c} \tag{3}$$

$$\alpha = \frac{1}{T_r^{0.5}} \tag{4}$$

The subscript c in Eqs. (2) and (3) stands for the values of the property at the critical point. The reduced temperature T_r is defined as the absolute temperature divided by the critical temperature (=T/

T_c). The critical properties of normal hydrogen can be found in the literature [47] as 32.98 K and 1.293 MPa for temperature and pressure, respectively.

2. Characteristics on Gaseous Hydrogen Flow

Compressibility is very important characteristic for analyzing fluid under flow. When a flow is compressible, the density of the fluid significantly changes along with streamlines, while incompressible flows do not exhibit such a variation of density. The key differentiation between compressible and incompressible flow depends on the relative velocity of the moving fluid. Usually, compressible flows are at high speeds with Mach number (Ma) greater than about 0.3, but slow flows are treated as incompressible even though the fluid is a gas when Ma is lower than 0.3 since the density change is less than 5%. Ma is a dimensionless quantity representing the ratio of flow velocity to the local speed of sound defined by

$$\mathrm{Ma}=\frac{\mathrm{u}}{\mathrm{c}} \tag{5}$$

where, u is the local flow velocity with respect to the boundaries and c is the speed of sound in the fluid medium.

The expression of *c* in a real compressible gas of which molecular weight is M_w can be written as [48]

$$\mathrm{C}^2=-\frac{\mathrm{C}_p}{\mathrm{C}_v}\frac{\mathrm{V}^2}{\mathrm{M}_w}\left(\frac{\partial \mathrm{P}}{\partial \mathrm{V}}\right)_T \tag{6}$$

where, C_p and C_v are the specific heat capacities at constant pressure and constant volume, respectively. RK EOS (Eq. (1)) can be used to obtain the partial derivative in Eq. (6), which becomes

$$\left(\frac{\partial \mathrm{P}}{\partial \mathrm{V}}\right)_T=-\frac{\mathrm{RT}}{(\mathrm{V}-\mathrm{b})^2}+\frac{\mathrm{a}(2\mathrm{V}+\mathrm{b})}{\mathrm{V}^2(\mathrm{V}+\mathrm{b})^2} \tag{7}$$

Therefore, the speed of sound in a real gas depends on temperature as well as pressure. Consequently, Ma also varies with temperature and pressure even under a constant mass flow rate. In Eq. (6), the temperature dependence of C_p/R is given by the following equation [47] and C_v is calculated by a relation between the two

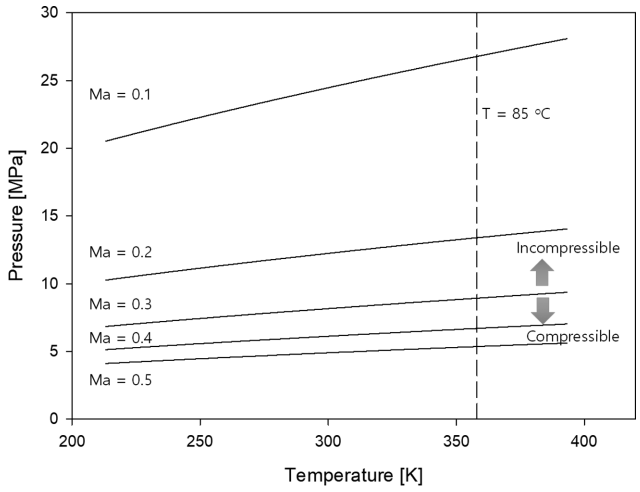

Fig. 4. Plots of Ma with temperature and pressure for 60 g/s mass flow rate through a schedule 80 1/4 inch pipe.

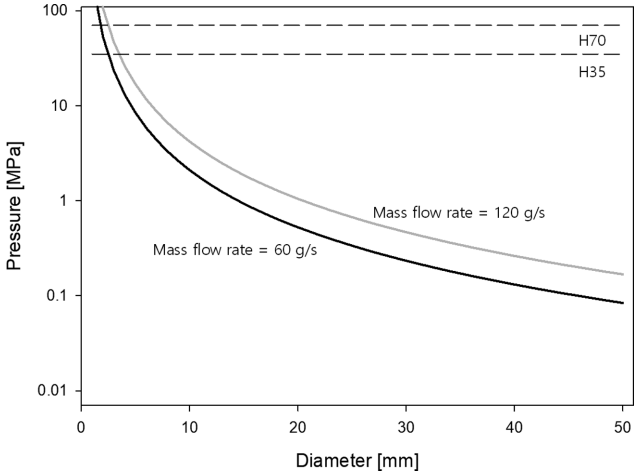

Fig. 5. Pressure profile with a diameter of a pipe representing Ma= 0.3 at −40 °C for two mass flow rate limits.

specific heat capacities ($C_v=C_p-R$):

$$\frac{\mathrm{C}_p}{\mathrm{R}}=2.883+3.681\times10^{-3}\mathrm{T}-0.772\times10^{-5}\mathrm{T}^2+0.692\times10^{-8}\mathrm{T}^3-0.213\times10^{-11}\mathrm{T}^4 \tag{8}$$

Fig. 4 presents calculated Ma values with respect to pressure and temperature when the mass flow rate is the maximum for LDVs (60 g/s) and the inside sectional area of a pipe is 5.0×10^{-4} ft^2, which is a typical value of a standard schedule 80 1/4 inch pipe.

The temperature and pressure regions to satisfy the incompressible flow condition is indicated in Fig. 4. It shows that the pressure on a flow should exceed around 7 MPa throughout the temperature range to be treated as an incompressible flow. However, Ma is in proportion to the mass flow rate and the maximum flow rate usually takes place at higher pressure than 7 MPa at a station side. The velocity of a flowing gas depends on not only temperature and pressure but the diameter of a pipe or a hose. Fig. 5 shows pressure profiles representing Ma=0.3 at −40 °C with a diameter of a pipe at two different mass flow rates, which are the maximum limits for LDVs and HDVs. The pressure region below the respective line falls in a compressible flow condition at each mass flow rate. Therefore, a proper design of HRS (H35 or H70) necessitates the consideration of a pipe size to obtain a stable incompressible flow throughout the refueling process. The larger the pipe diameter, the wider becomes the pressure range at HRSs. However, the size of a pipe should be determined based on the aspect of an optimization for station operation [36,49]. The temperature and pressure on the occurrence of the maximum flow rate depends on the operation method. A refueling process is usually controlled by one of two methods. In standard protocols such as SAE J2601, the pressure at a station is controlled and, thus, the mass flow rate is determined by the pressure difference between the station and the vehicle tank. On the other hand, the mass flow rate could be controlled instead and the pressure at the station is just monitored. Therefore, the station design, including the capacity of hydrogen storage, the capability of the pre-cooler, the diameter of the pipe and so on, should be associated with the operation method taken.

Table 1. Pressures [MPa] for Ma=0.3 with a diameter of a pipe and temperature at two different mass flow rates

Mass flow rate [g/s]	Diameter [mm]	Temperature [°C]				
		−40	−33	−26	−17.5	2.5
60	1	204.4051	207.7708	211.0822	215.0335	224.0501
	5	8.3787	8.5084	8.6362	8.7888	9.1378
	10	2.0980	2.1303	2.1620	2.2000	2.2869
	15	0.9325	0.9469	0.9610	0.9779	1.0165
	20	0.5246	0.5326	0.5406	0.5501	0.5718
	25	0.3357	0.3409	0.3460	0.3520	0.3659
120	1	411.3510	417.9769	424.5001	432.2891	450.0825
	5	16.6988	16.9611	17.2192	17.5274	18.2314
	10	4.1945	4.2591	4.3227	4.3988	4.5727
	15	1.8649	1.8936	1.9219	1.9556	2.0329
	20	1.0491	1.0652	1.0811	1.1001	1.1435
	25	0.6714	0.6818	0.6919	0.7041	0.7319

The pressures for Ma=0.3 at refueling temperatures are shown in Table 1. The temperatures in Table 1 are selected to present the classified station types (see Fig. 2). The effects of temperature on the pressure are not so significant when the temperature at station is maintained at the classified HRS temperatures. However, it is notable that a small diameter about <2 mm is not acceptable any of HRSs.

Flow patterns in the incompressible flow are categorized by well-known Reynolds number (Re), which is defined by the ratio of inertial resistance to viscous resistance for a flowing fluid. Re for an internal pipe flow is expressed as

$$\mathrm{Re}=\frac{\mathrm{Du}\rho}{\mu}=\frac{\mathrm{DG}}{\mu} \tag{9}$$

where, μ and ρ are viscosity and density of a fluid, respectively. D stands for diameter of a pipe and G for the mass flow rate per unit area.

As recognized in Eq. (9), Re solely depends on viscosity under a given mass flow rate at a specified pipe diameter. Viscosity of a gas is affected by temperature as well as pressure when the gas is highly compressed. Pressure has a strong effect on viscosity of pure gases at much higher pressures than a critical value. Therefore, a proper correlation for viscosity should be selected to take the effect of both temperature and pressure into consideration. Poling et al. [47] recommended the Lucas method be used to estimate viscosities of compressed gases at high densities. The method was developed to use temperature and pressure as the required properties to obtain the values of viscosity. Details of viscosity estimation are described in the Appendix.

The calculated Re under 60 g/s of the mass flow rate through a standard schedule 80 1/4 inch pipe is presented with temperature and pressure in Fig. 6. The minimum value is found at the highest pressure and temperature within the considered region and it is greater than 1.5×10^6, representing turbulent flow. During hydrogen refueling the lowest temperature and the highest pressure in a fueling line will be imposed on a refueling station because cooled and pressurized hydrogen is supplied from HRS to tanks in a vehicle. Therefore, turbulent flow could be assumed throughout the

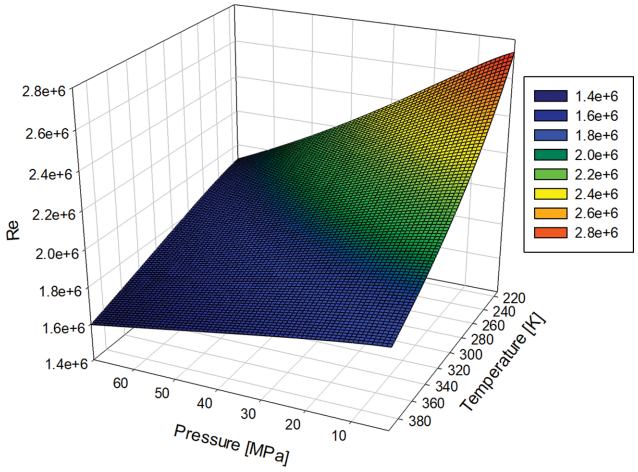

Fig. 6. Plot of Re with temperature and pressure for 60 g/s mass flow rate through a schedule 80 1/4 inch pipe.

fueling time. Re can also be calculated at different mass flow rates and diameters, but calculations under the other conditions are not given in the present paper since they have a linear effect on Re. It is expected that Re satisfies the turbulent condition (Re>>2300) under detectable mass flow rates.

During the hydrogen refueling process, the mass flow rate should not exceed the limits (60 and 120 g/s for LDVs and HDVs, respectively) to ensure safety. The maximum flow rates take place when the pressure difference between the station and the vehicle tank is the greatest. Therefore, it is required to estimate the pressure drop throughout a straight line, exhibiting the limit values on the mass flow rate. The pressure drop (ΔP) through a pipe length of L is expressed by the following equation:

$$\Delta P=2f_f\rho\frac{L}{D}u^2=2f_f\frac{L}{D}\frac{G^2}{\rho} \tag{10}$$

The Fanning friction factor (f_f) in Eq. (10) is a dimensionless number that can be obtained for turbulent flows in a smooth straight pipe by the following correlation equation with Re when $10^4<$

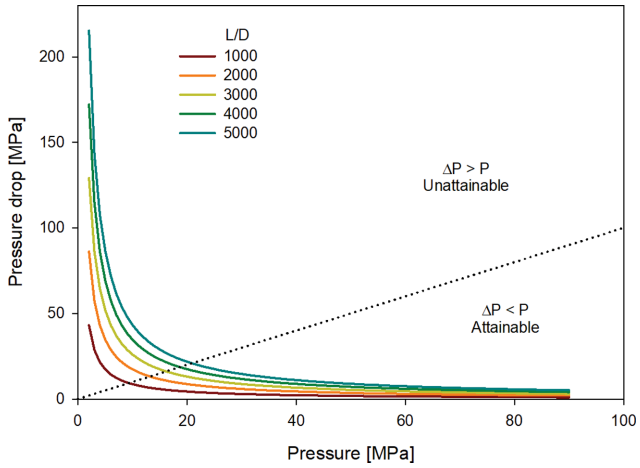

Fig. 7. Pressure drop (ΔP) variation with hydrogen suppling pressure (P) for 60 g/s mass flow rate at −40 °C through a 5 mm diameter pipe.

$Re<10^7$ [50]:

$$f_f = 0.0014 + \frac{0.125}{Re^{0.32}} \tag{11}$$

As for minor pressure losses, the equivalent length method using a L/D ratio allows to apply Eq. (11) for describing the pressure drop through fittings as a length of a straight pipe. Therefore, the effects of fittings on the pressure drop have not been explicitly considered and instead the pressure drop with respect to the length of a pipe was investigated at a hydrogen refueling condition.

The pressure drop estimated by Eq. (10) with hydrogen suppling pressure at T40 (T=−40 °C) is presented in Fig. 7 for 60 g/s mass flow rate and 5 mm diameter pipe. As pressure increases the density of a flowing fluid increases and, as a consequence, the pressure drop decreases at a given L/D value, which can be explained by Eq. (10). Fig. 7 is divided into two regions by a dotted line according to the comparison of pressure (P) with pressure drop (ΔP). Although ΔP can be calculated by equations at any given conditions, physically it cannot exceed the imposed P. The dotted line in Fig. 7 indicates ΔP=P. Therefore, the intersection of the dotted line and the pressure drop curve shows the minimum requirement to satisfy the flow rate of 60 g/s under the given conditions. For example, a pressure higher than 9.5 MPa should be imposed on HRS in order to obtain 60 g/s at −40 °C through a 5 mm pipe with L/D= 1,000. Table 2 presents the effects of refueling conditions such as the pre-cooled temperature and the length of gas flowing line, including hoses and pipes (see Fig. 1) on the minimum pressure required to obtain mass flow limits (60 or 120 g/s). The effect of temperature on the minimum pressure was found to be insignificant. Actually, pre-cooling is intended to keep the temperature of the hydrogen storage tank below the limit (85 °C for type IV tank) and the extent of pre-cooling is not closely associated with the flow characteristics. However, the effects of the diameter and the pipe length on the required pressure are considerable. The larger diameter and the shorter length are favorable for implementing maximum flow rates and thus reducing refueling time. Table 2 also indicates that it is inappropriate to use HRSs built for LDVs in refueling HDVs without increasing the pipe diameter since the imposed pressure drop would restrict the flow rate.

ANALYSIS OF HEAT TRANSFER THROUGH REFUELING LINE

1. Energy Balance and Heat Transfer Coefficient

The temperature of hydrogen entering an on-board storage tank becomes higher than the pre-cooled because of thermal interaction with the atmosphere along a flowing line. A gas in a line undergoes thermal interaction, as schematically described in Fig. 8. Adopting a lumped system assumption for the line which ignores temperature gradients radial and axial direction, the energy balance of the pipeline of inner diameter D_i, outer diameter D_o, and length L is expressed as the following equation:

$$\frac{dT_{pipe}}{dt} = \frac{4(q_o - q_i)}{C_{p,\,pipe}\rho_{pipe}(D_o^2 - D_i^2)\pi L} \tag{12}$$

Table 2. Minimum hydrogen suppling pressures [MPa] for attaining maximum mass flow rates through a pipe diameter D and length L

Mass flow rate [g/s]	Temperature [°C]	L [m]								
		2			4			6		
		D [mm]			D [mm]			D [mm]		
		5	8	10	5	8	10	5	8	10
60	−40	3.459	0.355	0.121	6.917	0.710	0.241	10.376	1.064	0.362
	−33	3.572	0.367	0.125	7.144	0.733	0.249	10.716	1.099	0.374
	−26	3.686	0.378	0.129	7.371	0.756	0.257	11.057	1.135	0.386
	−17.5	3.824	0.393	0.134	7.648	0.785	0.267	11.472	1.178	0.400
	2.5	4.152	0.426	0.145	8.304	0.853	0.290	12.456	1.279	0.435
120	−40	12.553	1.277	0.432	25.106	2.554	0.865	37.659	3.831	1.297
	−33	12.960	1.319	0.447	25.920	2.638	0.893	38.880	3.956	1.340
	−26	13.368	1.361	0.461	26.737	2.721	0.921	40.105	4.082	1.382
	−17.5	13.866	1.412	0.478	27.732	2.823	0.956	41.598	4.235	1.434
	2.5	15.043	1.532	0.519	30.085	3.064	1.038	45.128	4.597	1.557

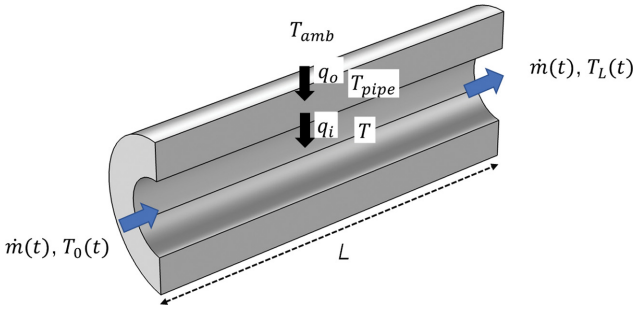

Fig. 8. Schematic diagram for thermal interaction through a pipe flowing hydrogen.

The outer heat flow rate (q_o) is associated with a respective heat transfer coefficient (h_o) as,

$$q_o = h_o(\pi D_o L)(T_{amb} - T_{pipe}) \tag{13}$$

where, T_{amb}, and T_{pipe} are temperature of the ambient and pipe, respectively.

The inner heat flow rate (q_i) can be calculated from the temperature increase of hydrogen from T_0 to T_L (see Fig. 8).

$$q_i = \dot{m} C_P (T_L - T_0) \tag{14}$$

Under an assumption of steady state at a constant wall temperature during a time step for a numerical calculation by the following equation derived from an energy balance of the flowing gas:

$$\ln\frac{T_L - T_{pipe}}{T_0 - T_{pipe}} + \frac{4L}{D_i}\frac{h_i}{GC_p} = 0 \tag{15}$$

The inner heat transfer coefficient (h_i) can be acquired from the skin friction factor using momentum-heat transfer analogies. Analogies have been widely adopted for the turbulent boundary layers because the transport of momentum and heat mostly depends on the same turbulent eddies. In this work, three well-known analogies expressing Stanton number (St) in terms of the friction factor (f_f) and Prandtl number (Pr) (see Table 3) [51-53] were examined to estimate the temperature of hydrogen exiting a pipeline. The two dimensionless numbers (St and Pr) in Table 3 are defined as,

$$St = \frac{h_i}{GC_p} \tag{16}$$

$$Pr = \frac{\mu C_p}{k} \tag{17}$$

where, k is the fluid thermal conductivity, which is also depending on temperature as well as pressure. In this work, we use a thermal conductivity correlation for normal hydrogen applicable up to 100 MPa [54].

2. Pipeline Outlet Temperature Calculation

The proposed temperature estimation model was compared with experimental data. There are not many experimental studies related to the heat transfer of hydrogen through pipes. Experimental data [29] of pipeline outlet temperature with respect to flow rate and inlet temperature for hydrogen refueling process were used to examine the effect of the parameters of the proposed model. The experimental conditions and pipeline (SUS316) specifications are summarized in Table 4.

The changes of inner heat transfer coefficient (h_i) calculated from three different analogy methods are compared and shown in Fig. 9 with Prandtl number (Pr) and friction factor (f_f). Throughout the hydrogen refueling, Pr is relatively stable at 0.7 while f_f decreases rapidly and remains stable at 3×10^{-3}. The Colburn analogy (CA) method estimates the largest values for h_i among the three methods. CA and vKA estimate about 20% and 7% higher values, respectively, than PA. However, it is found that the differences in the heat transfer coefficient estimated by the three analogy methods had

Table 3. Momentum-heat transfer analogies

Abbreviation	Analogy	Expression
CA	Colburn analogy [53]	$St = \frac{f_f}{2} Pr^{-2/3}$
PA	Prandtl analogy [51]	$St = \frac{f_f/2}{1 + 5\sqrt{f_f/2}(Pr - 1)}$
vKA	von Kármán analogy [52]	$St = \frac{f_f/2}{1 + 5\sqrt{f_f/2}\left\{Pr - 1 + \ln\left[1 + \frac{5}{6}(Pr - 1)\right]\right\}}$

Table 4. Summary of experimental conditions and pipeline specifications [29]

Experimental condition		Pipeline specification	
T_{amb} [°C]	0.0	D_i [mm]	4.53
T_0 [°C]	−40	D_o [mm]	9.53
Pressure ramp rate [MPa/min]	28.1	L [mm]	2,000
		ρ_{pipe} [kg/m^3]	7,900
		$C_{p,pipe}$ [J/(kg·K)]	590

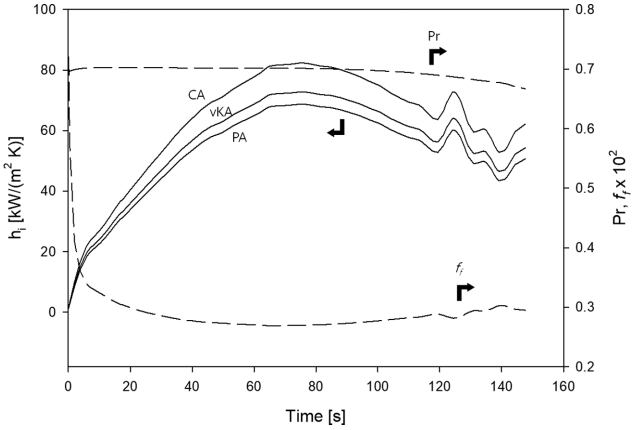

Fig. 9. Variations of inner heat transfer, Pr, and f_f with hydrogen refueling time.

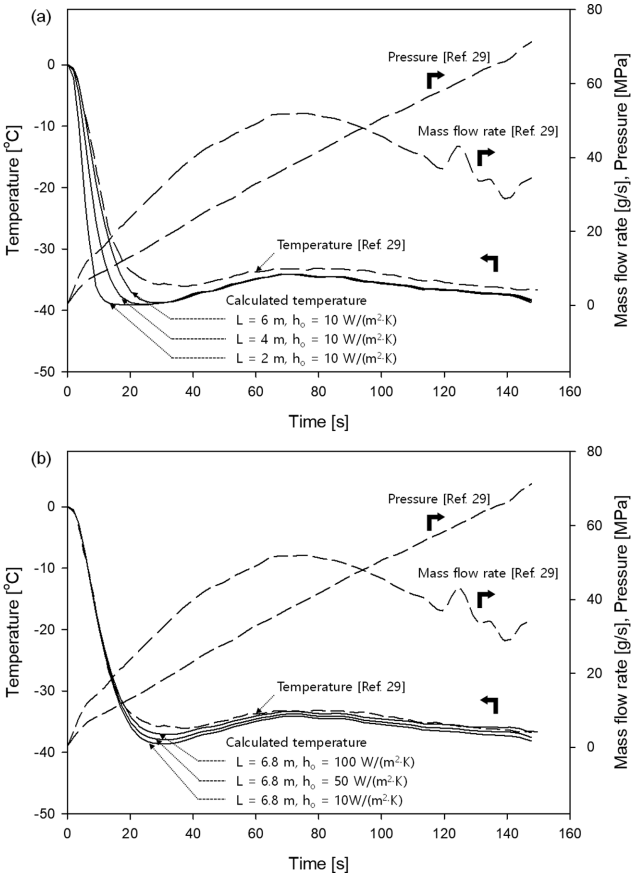

Fig. 10. Effect of model parameters on pipeline outlet temperature.

little effect on the hydrogen outlet temperature. The calculated temperature curves shown in Fig. 10(a) and (b) are superimposed on each other and indistinguishable regardless of the heat transfer coefficient estimation methods. The result is understood because the mass flow rate of hydrogen passing through a small-area pipe is quite large, so the effect of the difference of h_i in Eq. (15) does not appear significant The results of comparison with experimental data by changing the parameters used in the model are shown

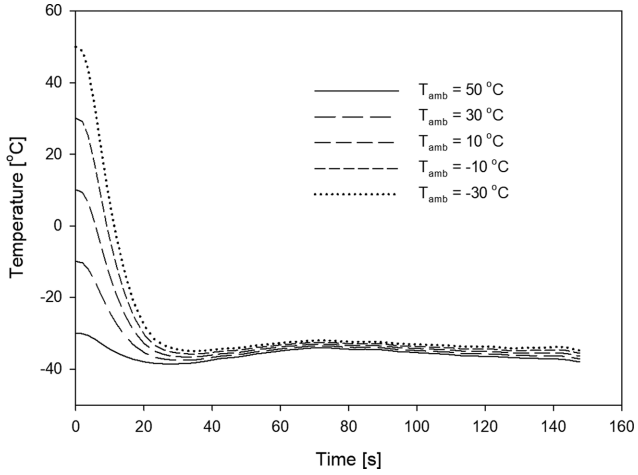

Fig. 11. Hydrogen outlet temperature changes with ambient temperature.

in Fig. 10.

The temperature of the outlet hydrogen drops sharply during the first 20 seconds and then remains stable at about −35 °C. Initially, the temperature of hydrogen is much higher than the pre-cooled temperature by thermal exchange with the pipeline, but it rapidly decreases due to the cooling of the pipeline as shown in Fig. 10. Fig. 10(a) is the result of comparing the temperature of hydrogen at the outlet of the pipeline, calculated by changing the length of the pipeline and using the suggested value in the literature [29] for the external heat transfer coefficient (h_o=10 W/(m^2·K)). The effect of the change of the external heat transfer coefficient at a constant pipeline length is shown in Fig. 10(b). The actual filling equipment consisted of various fittings such as elbow pipes, joints, and valves. Therefore, the thermal mass of the pipeline is greater than a straight line. In this work, the thermal mass was considered as the equivalent length. The increased length effects on the initial behavior (see Fig. 10(a)) but it does not change the stable temperature region. Fig. 10(b) presents the effect of the increased h_o at the constant length on the nearly steady state period. In this work, L=6.8 m and h_o= 100 W/(m^2·K) were determined to fit the experimental data.

SAE J2601, which is the most representative hydrogen refueling protocol, suggests an ambient temperature range of −40 to 50 °C and recommends no fueling beyond the range [3]. Using the parameters determined from the experimental data, the pipe outlet temperature changes within the range are calculated to present the effect of the ambient temperature. The calculation is carried out using the mass flow rate and pressure increase of the experiment (see Fig. 10) presented in the literature [29]. Fig. 11 shows the results in 20 °C increments from −30 to 50 °C. A small amount of hydrogen flows at the beginning of the refueling, and the hydrogen is easily heated by the tube at the ambient temperature. Therefore, the initial temperatures appear the same as the temperature of the pipe. As the pre-cooled hydrogen continues to flow into the pipe, the temperature of the pipe decreases and the temperature of the outlet hydrogen also decreases. Inner heat transfer actively occurs to raise the temperature of hydrogen during the initial 30 s, and after that, the pipe is sufficiently cooled to reach a steady state in

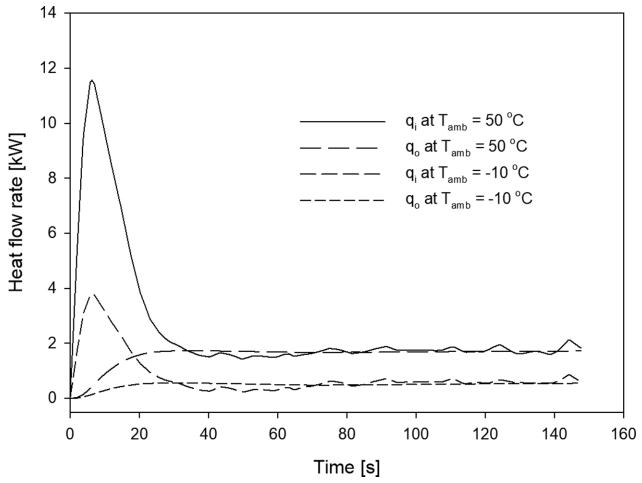

Fig. 12. Heat transfer rate changes at two temperatures.

Table 5. End temperature at pipe exit and averaged temperature increase of fueled hydrogen with ambient temperature

T_{amb} [°C]	$T_{L,end}$ [°C]	Accumulated heat added [kJ]	$\overline{\Delta T}$ [°C]
−30	−38.0	31.45	0.387
−10	−37.2	118.5	1.459
10	−36.4	205.6	2.532
30	−35.6	292.7	3.605
50	−34.8	379.8	4.677

which the outer heat transfer and inner heat transfer are balanced. The changes of the heat transfer rate (q_i and q_o) with time are compared in Fig. 12 for two ambient temperatures (−10 and 50 °C). As explained, q_i is significantly larger than q_o for 30 s, which causes the outlet hydrogen temperature to be relatively high. After the cooling of pipe is completed (t>30 s), the outer and the inner heat transfer rate get close to each other. The small fluctuations in the amount of the inner heat transfer that occur at t>30 s are due to the fluctuation of the mass flow rate. Table 5 shows the pipe outlet temperature at the end of refueling ($T_{L,end}$), the amount of heat added to hydrogen, and the average temperature rise ($\overline{\Delta T}$) of hydrogen based on the fueled mass with the ambient temperature. $\overline{\Delta T}$ is calculated by the following equation. In Eq. (18), the fueled mass (m) is 5.6 kg and the specific heat (C_p) is 14.5 kJ/kg·°C.

$$\overline{\Delta T} = \frac{1}{mC_p}\int q_i dt \tag{18}$$

It is found that for every 20 °C increase in ambient temperature, the average hydrogen temperature rises by about 1 °C. However, the results of this calculation depend on the experimental conditions. If the length of the pipe is increased or the filling time is increased, the temperature rise will increase, and vice versa, the temperature rise will decrease under actual refueling processes.

CONCLUSIONS

The flow characteristics under hydrogen refueling conditions were analyzed to estimate the heat transfer coefficient and a model for calculating the hydrogen temperature is proposed under the analysis result. Applying RK EOS and other correlation equations of real gases, incompressible flow conditions were estimated with the process conditions. It is identified that incompressible flow exhibits turbulent behavior. Based on equations for turbulent flow, the pressure drops that occur during flowing through a pipeline were calculated, and the heat transfer coefficients (h_i) inside the pipe were estimated. Three analogous methods (Colburn, Prandtl, and von Kármán) were examined to simulate experimental data. It is found that the Colburn analogy estimates the highest values on h_i. However, the differences observed in the values of h_i have little impact on the calculation results of the pipeline out temperature due to relatively high mass flow rate.

A straight-line assumption underestimates the thermal mass of a pipeline consisting of various fittings such as valves and elbows. Therefore, it is required to apply an equivalent length concept in the simulation. The extended length reflecting the fittings affects the initial temperature of the pipeline outlet temperature. However, during the period revealing a steady state, there is little effect of the lengthened pipeline, and it is found that the outlet temperature is properly simulated by the change of the external heat transfer coefficient. It is presumed that the increased external heat transfer coefficient reflects the frost formation occurring during the hydrogen charging process. Using the parameters fitted from experimental data, the effect of the ambient temperature was investigated to find that for every 20 °C increase in ambient temperature, the average hydrogen temperature rises by about 1 °C. However, the actual temperature increase depends on the actual process conditions.

ACKNOWLEDGEMENTS

This work was supported by the Korea Institute of Energy Technology Evaluation and Planning (KETEP) and the Ministry of Trade, Industry & Energy (MOTIE) of the Republic of Korea (No. 20192910100170).

REFERENCES

1. Y. Li and S. Kimura, *Energy Policy*, **148**, 111980 (2021).
2. T. Stangarone, *Clean Technol. Environ. Policy*, **23**, 509 (2021).
3. SAE Engineers, Fueling protocols for light duty gaseous hydrogen surface vehicles, SAE International (2020).
4. C. Cunanan, M.-K. Tran, Y. Lee, S. Kwok, V. Leung and M. Fowler, *Clean Technol.*, **3**, 474 (2021).
5. SAE Engineers, Fueling protocol for gaseous hydrogen powered heavy duty vehicles, SAE International (2014).
6. G. Xu, K. Pareek, N. Li and H. Cheng, *Int. J. Hydrogen Energy*, **40**, 16330 (2015).
7. K. Pareek, R. Rohan, Z. Chen, D. Zhao and H. Cheng, *Int. J. Hydrogen Energy*, **42**, 6801 (2017).
8. T. Hua, R. Ahluwalia, J.-K. Peng, M. Kromer, S. Lasher, K. McKenney, K. Law and J. Sinha, *Int. J. Hydrogen Energy*, **36**, 3037 (2011).
9. R. K. Ahluwalia, T. Hua and J. Peng, *Int. J. Hydrogen Energy*, **37**, 2891 (2012).
10. C. He, R. Yu, H. Sun and Z. Chen, *Int. J. Hydrogen Energy*, **41**, 15812

(2016).
11. M. Li, Y. Bai, C. Zhang, Y. Song, S. Jiang, D. Grouset and M. Zhang, *Int. J. Hydrogen Energy*, **44**, 10677 (2019).
12. S. Maus, J. Hapke, C. N. Ranong, E. Wüchner, G. Friedlmeier and D. Wenger, *Int. J. Hydrogen Energy*, **33**, 4612 (2008).
13. R. O. Cebolla, B. Acosta, P. Moretto and N. De Miguel, *Int. J. Hydrogen Energy*, **44**, 8601 (2019).
14. R. O. Cebolla, B. Acosta, P. Moretto, N. Frischauf, F. Harskamp, C. Bonato and D. Baraldi, *Int. J. Hydrogen Energy*, **39**, 6261 (2014).
15. B. Acosta, P. Moretto, N. de Miguel, R. Ortiz, F. Harskamp and C. Bonato, *Int. J. Hydrogen Energy*, **39**, 20531 (2014).
16. T. Bourgeois, F. Ammouri, M. Weber and C. Knapik, *Int. J. Hydrogen Energy*, **40**, 11748 (2015).
17. C. J. B. Dicken and W. Merida, *Numer. Heat Transf.; A: Appl.*, **53**, 685 (2007).
18. L. Zhao, Y. Liu, J. Yang, Y. Zhao, J. Zheng, H. Bie and X. Liu, *Int. J. Hydrogen Energy*, **35**, 8092 (2010).
19. S. C. Kim, S. H. Lee and K. B. Yoon, *Int. J. Hydrogen Energy*, **35**, 6830 (2010).
20. I. Simonovski, D. Baraldi, D. Melideo and B. Acosta-Iborra, *Int. J. Hydrogen Energy*, **40**, 12560 (2015).
21. J. Zhang, T. S. Fisher, P. V. Ramachandran, J. P. Gore and I. Mudawar, *J. Heat Transfer*, **127**, 1391 (2005).
22. J. C. Yang, *Int. J. Hydrogen Energy*, **34**, 6712 (2009).
23. C. N. Ranong, S. Maus, J. Hapke, G. Fieg and D. Wenger, *Heat Transfer Engineering*, **32**, 127 (2011).
24. F. Olmos and V. I. Manousiouthakis, *Int. J. Hydrogen Energy*, **38**, 3401 (2013).
25. E. Ruffio, D. Saury and D. Petit, *Int. J. Hydrogen Energy*, **39**, 12701 (2014).
26. P. L. Woodfield, M. Monde and Y. Mitsutake, *J. Therm. Sci. Technol.*, **2**, 180 (2007).
27. P. L. Woodfield, M. Monde and T. Takano, *J. Therm. Sci. Technol.*, **3**, 241 (2008).
28. M. Heath, P. L. Woodfield, W. Hall and M. Monde, *Exp. Therm Fluid Sci.*, **54**, 151 (2014).
29. T. Kuroki, N. Sakoda, K. Shinzato, M. Monde and Y. Takata, *Int. J. Hydrogen Energy*, **43**, 1846 (2018).
30. J. Xiao, P. Bénard and R. Chahine, *Int. J. Hydrogen Energy*, **41**, 5531 (2016).
31. J. Xiao, X. Wang, X. Zhou, P. Bénard and R. Chahine, *Int. J. Hydrogen Energy*, **44**, 8780 (2019).
32. S. Deng, J. Xiao, P. Bénard and R. Chahine, *Int. J. Hydrogen Energy*, **45**, 20525 (2020).
33. J. Liu, S. Zheng, Z. Zhang, J. Zheng and Y. Zhao, *Int. J. Hydrogen Energy*, **45**, 9241 (2020).
34. R. Caponi, A. M. Ferrario, E. Bocci, G. Valenti and M. Della Pietra, *Int. J. Hydrogen Energy*, **46**, 18630 (2021).
35. K. Reddi, A. Elgowainy and E. Sutherland, *Int. J. Hydrogen Energy*, **39**, 19169 (2014).
36. L. Viktorsson, J. T. Heinonen, J. B. Skulason and R. Unnthorsson, *Energies*, **10**, 763 (2017).
37. A. Mayyas and M. Mann, *Int. J. Hydrogen Energy*, **44**, 9121 (2019).
38. J. O. Valderrama, *Ind. Eng. Chem. Res.*, **42**, 1603 (2003).
39. N. Sakoda, K. Shindo, K. Shinzato, M. Kohno, Y. Takata and M. Fujii, *Int. J. Thermophys.*, **31**, 276 (2010).
40. K. Nasrifar, *Int. J. Hydrogen Energy*, **35**, 3802 (2010).
41. M. C. Galassi, D. Baraldi, B. A. Iborra and P. Moretto, *Int. J. Hydrogen Energy*, **37**, 6886 (2012).
42. D. Melideo and D. Baraldi, *Int. J. Hydrogen Energy*, **40**, 735 (2015).
43. D. Melideo, D. Baraldi, B. Acosta-Iborra, R. O. Cebolla and P. Moretto, *Int. J. Hydrogen Energy*, **42**, 7304 (2017).
44. S. Sapre, K. Pareek, R. Rohan and P. K. Singh, *Energy Storage*, **1**, e91 (2019).
45. B. H. Park, *Trans. Korean Hydrogen New Energy Soc.*, **31**, 184 (2020).
46. P. J. Linstrom and W. G. Mallard, *J. Chem. Eng. Data*, **46**, 1059 (2001).
47. B. E. Poling, J. M. Prausnitz and J. P. O'connell, *The properties of gases and liquids*, McGraw-Hill, New York (2001).
48. X. Ma, X. Tang, Z. Wang, Q. Wang and D. Gao, *Sci. Rep.*, **10**, 1 (2020).
49. A. Elgowainy, K. Reddi, E. Sutherland and F. Joseck, *Int. J. Hydrogen Energy*, **39**, 20197 (2014).
50. G. E. Klinzing, F. Rizk, R. Marcus and L. Leung, *Pneumatic conveying of solids: A theoretical and practical approach*, Springer Science & Business Media (2011).
51. F. W. Dittus, *Univ. Calif. Pubs. Eng.*, **2**, 443 (1930).
52. T. V. Karman, *Transactions of the American Society of Mechanical Engineers*, **61**, 705 (1939).
53. A. P. Colburn, *Trans. Am. Inst. Chem. Engrs.*, **29**, 174 (1993).
54. S. Moroe, P. Woodfield, K. Kimura, M. Kohno, J. Fukai, M. Fujii, K. Shinzato and Y. Takata, *Int. J. Thermophys.*, **32**, 1887 (2011).

APPENDIX

At low pressure, the reduced inverse viscosity ξ is estimated by the following equation:

$$\xi = 0.176\left(\frac{T_c}{M_w^3 P_c^4}\right)^{1/6} \tag{A1}$$

The factor F_Q^0 is used for hydrogen, which is a function of a reduced temperature.

$$F_Q^0 = 1.22(0.76)^{0.15}\{1+0.00385[(T_r-12)^2]^{1/M_w}\,\mathrm{sign}(T_r-12)\} \tag{A2}$$

where sign in Eq. (A2) indicates +1 or −1 depending on whether the value of the argument is greater than zero or less than zero.

Two parameters, Z_1 and Z_2, are introduced to calculate viscosity. Z_2 is expressed as Eq. (A4) if $1<T_r<0$ and $0<Pr\leq 100$.

$$Z_1 = [0.807T_r^{0.618} - 0.357\exp(-0.449T_r) + 0.340\exp(-4.058T_r) + 0.018]F_Q^0 \tag{A3}$$

$$Z_2 = Z_1\left[1+\frac{aP_r^e}{bP_r^f + (1+cP_r^d)^{-1}}\right] \tag{A4}$$

The pressure correlation terms in Eq. (A4) are defined by the following equations:

$$a = \frac{1.245\times 10^{-3}}{T_r}\exp(5.1726T_r^{-0.3286}) \tag{A5}$$

$$b = a(1.6553T_r - 1.2723) \tag{A6}$$

$$c = \frac{0.4489}{T_r}\exp(3.0578T_r^{-37.7332}) \tag{A7}$$

$$d = \frac{1.7368}{T_r}\exp(2.2310T_r^{-7.6351}) \quad \text{(A8)}$$

$$e = 1.3088 \quad \text{(A9)}$$

$$f = 0.9425\exp(-0.1853T_r^{0.4489}) \quad \text{(A10)}$$

The correction factors F_Q is obtained by the ratio of Z_2 to Z_1.

$$Y = \frac{Z_2}{Z_1} \quad \text{(A11)}$$

$$F_Q = \frac{1+(F_Q^0-1)[Y^{-1}-0.007(\ln Y)^4]}{F_Q^0} \quad \text{(A12)}$$

Finally, the dense gas viscosity is calculated as

$$\mu = \frac{Z_2 F_Q}{\xi} \quad \text{(A13)}$$